This article has been accepted for publication in a future issue of this journal, but has not been fully edited. Content may change prior to final publication. Citation information: DOI 10.1109/TCPMT.2018.2875460, IEEE Transactions on Components, Packaging and Manufacturing Technology

Cu-Cu Bonding in Ambient Environment by Ar/N_2 Plasma Surface Activation and Its Characterization

Shen Lin Chua, Jiawei Marvin Chan, Simon Chun Kiat Goh and Chuan Seng Tan

***Abstract*— Ar/N_2 plasma surface activation in ambient environment for Cu-Cu bonding has been performed and characterized. Cu-Cu bonding occurs at room temperature and under normal atmospheric conditions. Post-bonding annealing is performed at 300 °C and below to control the overall thermal budget. Shear strength and hermeticity property of samples with varying annealing temperature are investigated. Samples annealed at 250 °C demonstrates the highest average shear strength of 20.3 MPa and lowest average helium leak rate of 8.7 × 10-9 atm.cc/s. Daisy chain structures are used to examine the electrical property of sample bonded at 300 °C and temperature cycling tests from -40 to 125 ºC for 1,000 cycles have been performed for reliability assessment. It is observed that the dies are well bonded and intact after 1,000 cycles even though the exposed Cu surface is heavily oxidized.**

***Index Terms*— Bonding processes, Packaging, Seals, Annealing, Bonding forces**

I. Introduction

With the applications of the internet of things (IoT) projected to grow in the years to come, the demand for smaller form factor packaged devices with multiple functionalities continues to increase. Devices for IoT typically consist of sensors, processors and communication chips packaged together in a small form factor [1]. This requires system scaling, increase in the number of components and complexity in each device, which in turn increases the interconnect density [2]. Hence, packaging technology with high density and low power consumption interconnects is required to connect individual components such that signal transmission and power delivery can be accomplished seamlessly. One of the promising technologies to package components in IoT devices is three-dimensional (3D) integration. 3D integration reduces the overall system form factor, propagation delay, energy consumption, and allows integration of heterogeneous components in a seamless way [3].

Solder-less metal bonding is widely used in 3D integration to form the connections between components for signal and power delivery. Examples of metal bonding include Au-Au, Al-Al, Au-Sn, Au-In and Cu-Cu bonding [4, 5, 6, 7 and 8]. Cu-Cu metal bonding was used in this study as Cu is commonly used as metallization layers in modern integrated circuits. This allows the ease of acceptance of this technology with the existing fabrication processes. Different Cu-Cu bonding methods have been studied in several studies such as thermo-compression bonding, direct Cu surface activated bonding (SAB), and direct Cu bonding with optimized chemical and mechanical polishing (CMP) [8, 9 and 3]. Among these methods, thermo-compression Cu bonding has the least stringent requirement for surface roughness of the Cu bonding layer. However, this method requires simultaneous application of external force and heating for a long duration during the entire bonding process [8]. If the surface roughness can be kept low (e.g., root mean square roughness below 1 nm), direct Cu SAB can be achieved in principle. In direct Cu SAB, initial bonding is achieved instantly, and this is followed by annealing to enhance the bond strength which can be accomplished in batches, hence resulting in shorter overall processing time (hence higher throughput) as compared to thermos-compression bonding. However, direct Cu SAB requires the alignment and bonding to be performed without breaking the high vacuum ($< 3 \times 10^{-3}$ Pa) and can only be done in a modified machine in most cases [9]. Direct Cu bonding with optimized CMP modifies the Cu surface and allows the bonding to take place in atmospheric ambient within a window of time lag after CMP [3]. The advantage of this bonding method is that it can be processed using existing semiconductor fabrication equipment.

In this study, Ar/N_2 plasma is used for surface activation of the Cu instead of CMP with similar advantages. Besides wafer to wafer bonding, this method can be extended to die level bonding to optimize the wafer usage when there is large size disproportion between the top and bottom die. The Ar/N_2 plasma activation method can also allow easier implementation of bonding of wafers fabricated externally as the CMP process does not need to be repeated. To evaluate the technical merits

This work was partially supported by Agency for Science, Technology and Research (A*STAR) under Grant # A1685b0005 and #A1783c0004

S. L. Chua is with the Nanyang Technological University, 50 Nanyang Ave, Singapore 639798 (e-mail: CH0028IN@e.ntu.edu.sg).

J. M. Chan is with the Nanyang Technological University, 50 Nanyang Ave, Singapore 639798 (e-mail: CHAN0731@e.ntu.edu.sg).

S. C. K. GOH is with the Nanyang Technological University, 50 Nanyang Ave, Singapore 639798 (e-mail: GOHC0075@e.ntu.edu.sg).

C. S. Tan is with the Nanyang Technological University, 50 Nanyang Ave, Singapore 639798 (e-mail: TanCS@ntu.edu.sg)

of Ar/N_2 plasma activation method for 3D integration, the physical properties of the bonded Cu are characterized. These properties include mechanical, hermeticity and electrical properties which are the primary considerations. The samples used in this study are prepared in the die form and bonded by Cu-Cu bonding using Ar/N_2 activation in atmospheric environment.

II. Plasma Activation

The Cu-Cu bonding method used in this study can be summarized in three steps. Figure 1 shows the three steps of plasma activation bonding process. The first step is to modify the Cu surface by physically removing surface copper oxides and impurities which are detrimental to bonding with plasma exposure. The second step is to place the bonding surfaces in proximity and apply sufficient force in ambient conditions to ensure uniform contact between the surfaces in order to initiate bonding. A commercial die bonder was used during this step. The last step is post-bonding batch annealing with no applied force to enhance the bonding strength by promoting Cu diffusion and grain growth across the bonding interface.

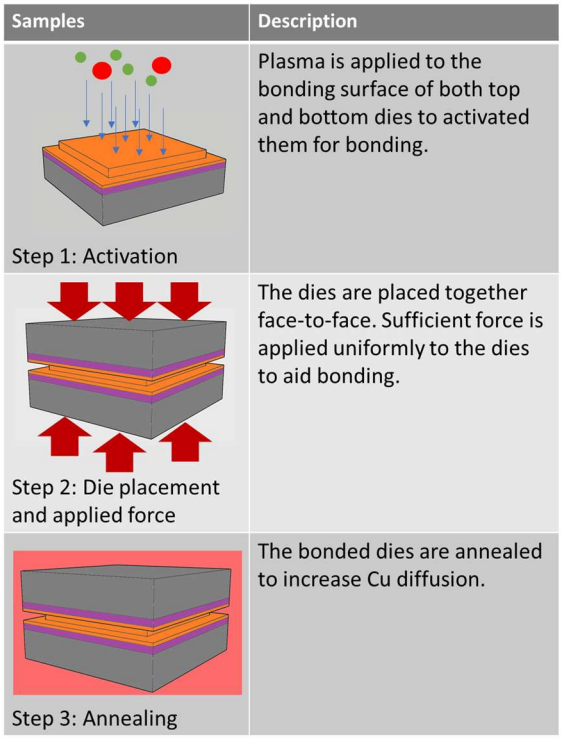

Fig. 1. Schematic of Cu-Cu plasma activation bonding method.

In the first step, either Ar/N_2 plasma or Ar plasma can be used to remove surface copper oxides and impurities. To determine which plasma best serves the purpose, the effects of Ar/N_2 and Ar plasma on the Cu surface was evaluated. For the purpose of evaluation, a 6" Si (100) wafer of 675µm thickness was deposited with 200 nm of SiO_2 by tetraethoxysilane (TEOS) plasma enhanced chemical vapor deposition (PECVD). The layer of SiO_2 was deposited to electrically isolate the Cu metal layer from the Si substrate. After the deposition of SiO_2, 100 nm Cu metal layer with 10 nm Ti barrier layer were deposited by e-beam evaporation physical vapor deposition (e-beam PVD). Subsequently, the wafer was diced into square dies with dimensions of 25.4 mm × 25.4 mm. Twelve dies were annealed for 1 h at 300 °C in vacuum (20 Pa) to stabilize the microstructure of the Cu layer. This annealing step will minimize variation in resistance due to grain size change in the Cu layer. The sheet resistance of the samples was measured before and after annealing. The average sheet resistance was 0.31 Ω/sq before and 0.29 Ω/sq after annealing. These samples were divided into 3 groups, and each group was subjected to Ar/N_2 plasma activation, Ar plasma activation and no activation. The parameters of Ar/N_2 plasma activation and Ar plasma activation are shown in Table I. Both plasma activation uses Ar only for cleaning of the Cu surface. After the plasma activation, the samples were annealed for 2 h at 300 °C (the highest temperature to be used for annealing in this study) in N_2 environment. After annealing, the sheet resistance of the samples was measured to examine the effects of activation on the electrical property.

Table I. Parameters of Plasma Activation

Cleaning Step	Similar for Both Activation	
Time	7 s	
Pressure	20 Pa	
RF Power	200 W	
Ar Gas Flow	100 cm^3/min	
Activation Step	Ar/N_2	Ar
Time	10 s	
Pressure	20 Pa	
RF Power	200 W	
Ar Gas Flow	50 cm^3/min	150 cm^3/min
N_2 Gas Flow	100 cm^3/min	0 cm^3/min

The variation of sheet resistances of the Cu layer after annealing is shown in Figure 2. Ar/N_2 plasma activated and non-activated samples show small increase of sheet resistance (5.8 and 4.3% respectively). However, Ar plasma activation results in significant increase of sheet resistance in the Cu layer (33.3%). The increase in the sheet resistance after annealing is due to unintentional surface oxidation during annealing as the N_2 chamber contains residual O_2. Plasma activation creates a highly energized Cu surface causing it to oxidize readily at a higher rate than a non-activated surface. Hence, the Ar plasma activated surface samples have higher sheet resistances after annealing. In the case of Ar/N_2 plasma activation, the activation was found to form a layer of copper nitride on the Cu surface in previous work [10]. Due to its inert property, the copper nitride needs to decompose before the Cu surface starts to oxidize. This reduces the oxidation rate of the Cu surface in the presence of a copper nitride passivation layer and hence a smaller increase in sheet resistances. Therefore, Ar/N_2 plasma was selected to activate the surfaces in Cu direct bonding in this study.

This article has been accepted for publication in a future issue of this journal, but has not been fully edited. Content may change prior to final publication. Citation information: DOI 10.1109/TCPMT.2018.2875460, IEEE Transactions on Components, Packaging and Manufacturing Technology

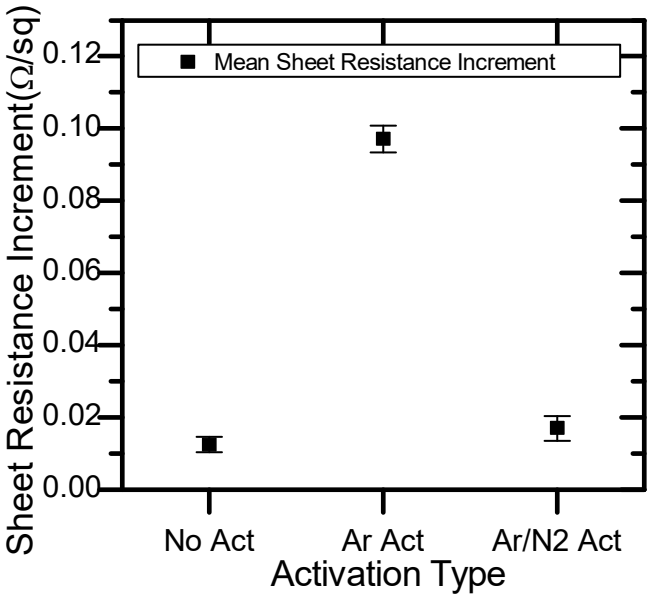

Fig. 2. Mean increase in sheet resistance after annealing at 300 ºC for different activation conditions.

III. Wafer to Wafer Bonding

A. Experimental Procedure

Blanket wafer to wafer bonding was performed to demonstrate Cu-Cu bonding with the Ar/N_2 plasma activation. Two 6" Si wafers (100) of 675 µm thickness were deposited with 10nm of Ti as adhesion/barrier layer and 100 nm of Cu using e-beam PVD. After the metal layers were deposited, both wafers were activated by Ar/N_2 plasma with the parameters stated in Table 1. After activation, the wafers were placed together in a double-sided wafer aligner vacuum contact mode for 4 min. Lastly, the bonded wafers were sent for post-bonding annealing at 300 ºC for 2 h in N_2 environment. The annealed wafers were diced into 10 mm by 10 mm square dies. Transmission electron microscopy (TEM) image and electron energy loss spectroscopy (EELS) analysis were performed in a previous study and concluded successful Cu-Cu bonding [11]. To study the reliability of the Cu-Cu bonding with the Ar/N_2 plasma activation, the dies were sent for temperature cycling test (TCT) of 1000 cycles ranging from -40 to 125 ºC in atmospheric environment.

B. Results and Discussion

Figure 3 and 4 shows the TEM image and EELS mapping of a TCT sample respectively. Focus ion beam (FIB) were used for sample preparation. There were no voids at the bonding interface observable in the TEM images and O and N were not observed in the EELS mapping. This showed that there were no degradations of the Cu-Cu bonding interface caused by 1000 cycles of TCT. Unlike Sn-Ag-Cu solder on Cu pillar, there were no voids [12] at the Cu bonding interface as there was no intermetallic compound changes could cause volume change.

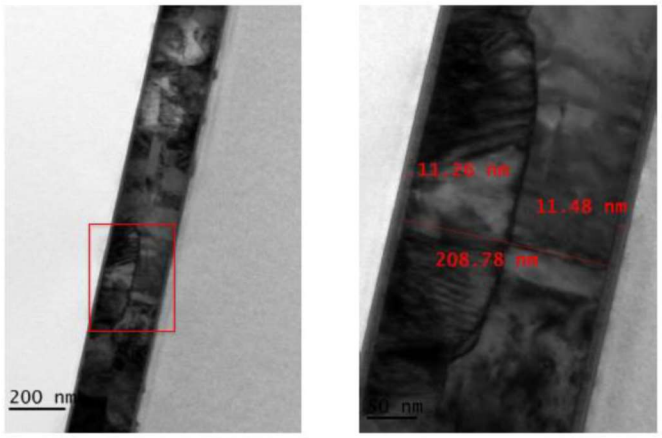

Fig. 3. TEM image of bonded sample after 1000 TCT with 200 nm and 50 nm scale bar respectively.

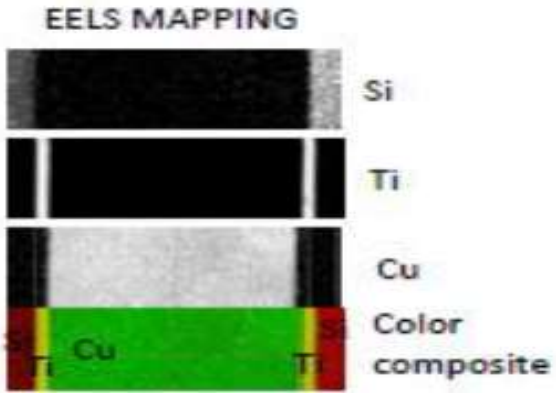

Fig. 4. EELS mapping of bonded sample after 1000 TCT showing Si, Ti and Cu.

IV. Cu-Cu Bonds Mechanical Property

A. Experimental Procedure

To characterize the mechanical properties of the bonded Cu after Ar/N_2 plasma activation, shear strength test was used to obtain the shear strength of the bonded samples. The top and bottom dies were prepared as shown in Figure 5. Two 6" Si wafers (100) of 675µm thickness were used as the substrates for the top and bottom dies. Reactive-ion etching (RIE) was used to etch 6 µm of Si on the wafer for the top dies. This is to provide a gap at the edge between the top and bottom dies such that subsequent dicing step will not affect the bonded interface. The 1.5 mm by 1.5 mm square feature of the top die defines the bonding area as shown in Figure 5. After RIE to define the top dies, 200 nm SiO_2, 10 nm Ti and 100 nm Cu was deposited on both wafers. Subsequently, the wafers were diced into 2 mm by 2 mm dies. Each pair of top and bottom dies for shear strength test was activated by Ar/N_2 plasma. Figure 6 shows the atomic force microscopy (AFM) scan of an activated sample and Figure 7 shows the 3D image of the 10 µm × 10 µm scanned area. The average root mean square (RMS) roughness of the activated samples is 1.17 nm. Figure 8 shows a profiler linescan of the surface of an activated sample. High height variations can be observed from the profiler linescan which increases the bonding force required. Within 3 min of activation, the top and bottom die were placed face to face and a bonding force of 375

N was applied to each pair of dies for 5 min to ensure good and uniform contact between the bonding surfaces. The bonded samples were subjected to post-bonding annealing with no applied force.

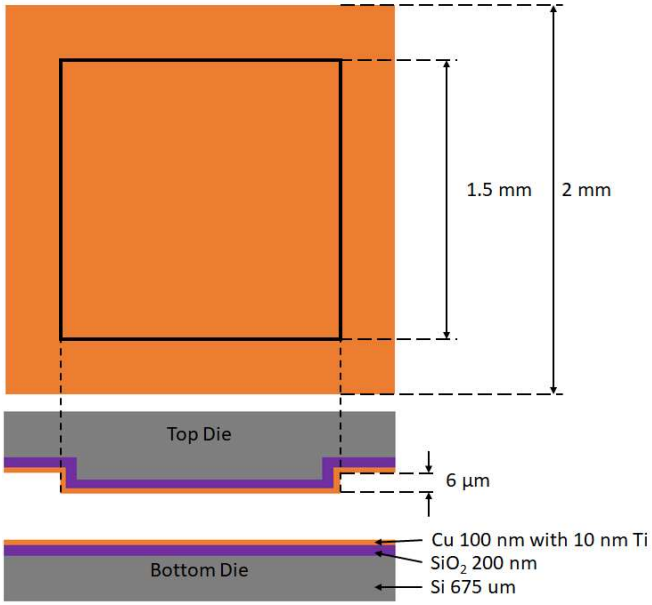

Fig. 5. Schematics of the top and bottom dies for shear strength test samples

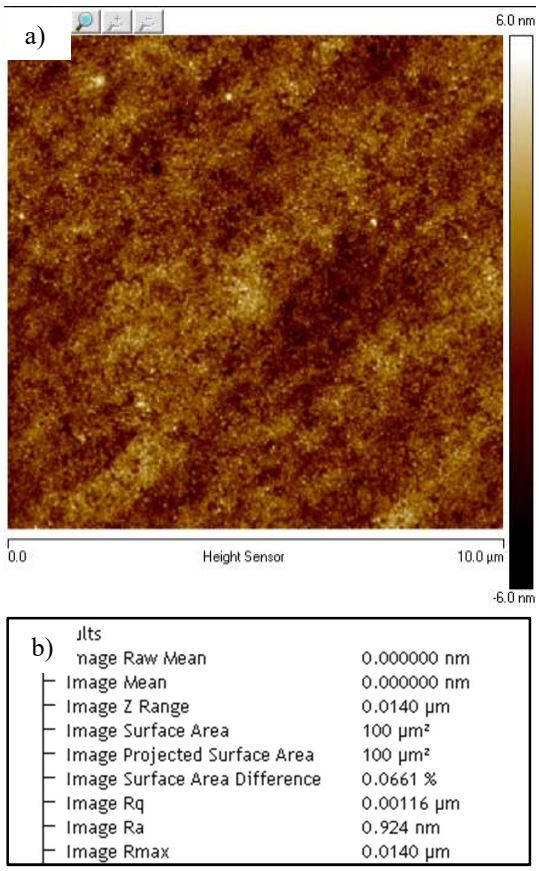

Fig. 6. AFM (10 µm ×10 µm) of activated sample showing a) 2D height map, b) roughness values

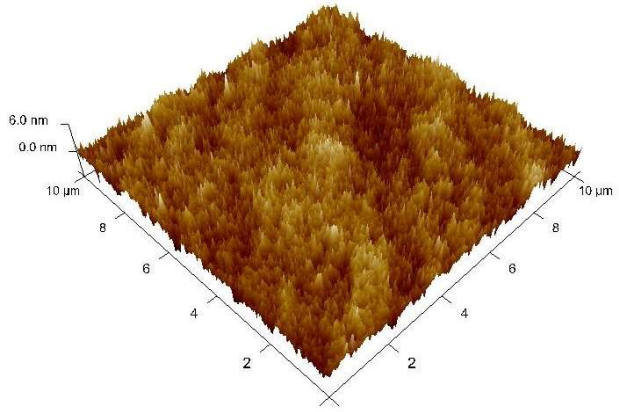

Fig. 7. AFM (10 µm ×10 µm) 3D height image of activated sample.

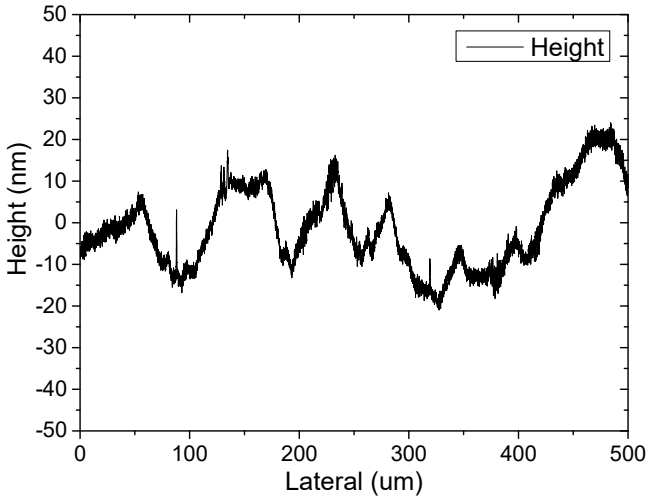

Fig. 8. Profiler linescan of activated sample showing height variations over 500 µm scan length.

Initially when the activated Cu surfaces were brought in contact, only small areas were in contact due to the roughness and unevenness of the surface (i.e. surface asperity). The local contact stress greatly exceeded the yield point of Cu and deform plastically, increasing the area of contact until the contact stress falls below the yield point of Cu. Due to low roughness of the surface when compared to thermocompression bonding, majority of the top and bottom surface were close enough together for the Van der Waals force to bond them together. This allowed the removal of force applied on the dies unlike thermocompression bonding. Next, post-bonding annealing was performed to strengthen the Cu bonds. The temperature used for the post-bonding annealing needs to be kept at 300 ºC and below to prevent undesired damage to the CMOS devices in actual manufacturing. As the annealing temperature was considerably lower than the melting point of Cu, grain boundary self-diffusion is the most dominant mechanism of self-diffusion [13]. Initially, surface diffusion occurred at the voids at the bonding interface due to chemical potential from different curvature at different part of each void [14]. Surface diffusion reduced the size of the voids and turned irregular voids into spherical voids. However, once the voids become spherical, surface diffusion greatly reduced. At this point, diffusion across the interface boundary became the most

This article has been accepted for publication in a future issue of this journal, but has not been fully edited. Content may change prior to final publication. Citation information: DOI 10.1109/TCPMT.2018.2875460, IEEE Transactions on Components, Packaging and Manufacturing Technology

dominant mechanism. Since interface boundary can be treated as normal grain boundary, diffusion across the interface can be considered as grain boundary diffusion [14]. Grain boundary self-diffusion follows the Arrhenius relation as shown in Equation 1. In the equation, D_b represent the grain boundary diffusion coefficient, δ the boundary thickness, $(\delta D_b)_0$ the pre-exponential factor, Q_b the activation energy, R the universal gas constant and T is the absolute temperature. The δD_b used in this study was obtained with values of $(\delta D_b)_0$ and Q_b from a study by Gust et al. [15].

$$\delta D_b = (\delta D_b)_0 \exp(-Q_b/RT) \quad \text{(Eq. 1)}$$

The values for δD_b for temperature 100 to 350 ºC (373 to 623 K) are presented in Figure 9 and it can be observed that δD_b decreases from 7.8 to 21.0 times for each 50 ºC decrement from 300 to 150 ºC (573 to 423 K). Increase in annealing temperature will have the greater effect on diffusion than that of increase in annealing time. Therefore, only variation in the annealing temperature on the shear strength test was investigated. Post-bonding annealing was performed at 150 ºC with 50 ºC increments to 300 ºC in this study.

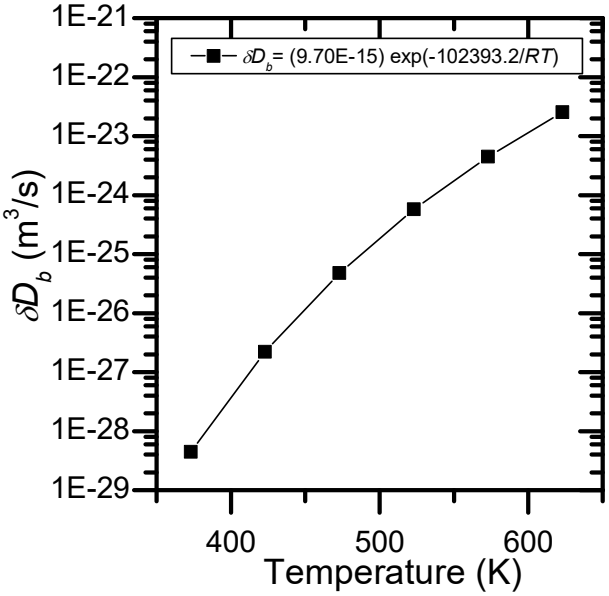

Fig. 9. Plot of δD_b using $(\delta D_b)_0$ and Q_b from Gust *et al.* with temperature from 373 to 623K

A set of 10 samples was prepared for each annealing temperature. The entire duration of temperature ramping and holding time was kept the same for the different annealing temperatures as shown in Figure 10. For example, the holding time was 2 h for post-bonding annealing at 300 ºC. After post-bonding annealing, the samples were sheared in order to estimate their shear strength.

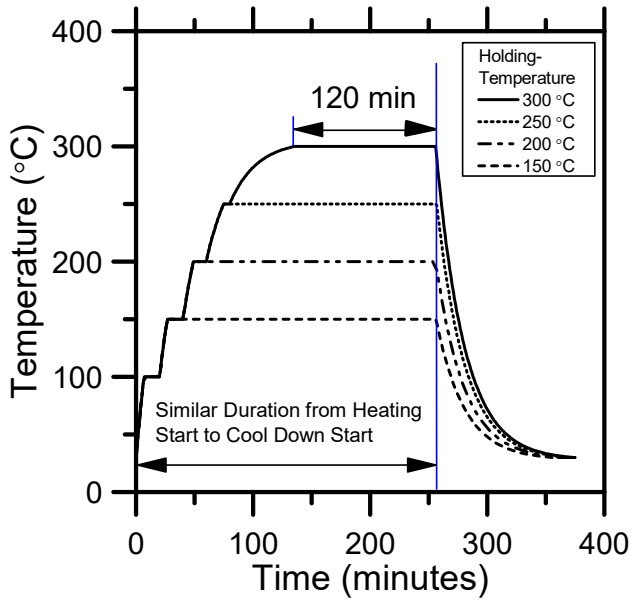

Fig. 10. Profile for different annealing temperature. The holding time for 300 ºC is 120 min.

B. Results and Discussion

In Figure 11, the shear strength test results show that the samples annealed at 250 ºC have the highest shear strength on average while those annealed at 150 ºC have the lowest average shear strength. It can also be observed that the shear strength increases with the increase of post-bonding annealing temperature up to 250 ºC. This is due to the higher grain boundary diffusion at higher temperature which promotes diffusion and grain growth across the bonding interface hence forming a stronger bond. However, the samples annealed at 300 ºC have lower shear strength as compared to 250 ºC annealed samples despite higher amount of grain boundary diffusion. Careful observation of the sheared samples concluded that failure of the samples occurred at the Ti layer as there was no Cu-Cu interface failure for the samples annealed at 250 and 300 ºC. The lower shear strength of the 300 ºC annealed sample could be attributed to higher amount of oxidation of the Ti barrier layer. This oxidation of Ti layer can be attributed to the high affinity of Ti for oxygen that decomposes the SiO_2 to form TiO_2 [16, 17]. The lower temperature annealed samples (150 to 200 ºC) have mixed failure interface where each sample failed at both the Cu-Cu interface and at the Ti layer. This is attributed to the lower rate of Cu self-diffusion and hence a weaker Cu-Cu bonding strength that succumbs to mechanical shear force.

This article has been accepted for publication in a future issue of this journal, but has not been fully edited. Content may change prior to final publication. Citation information: DOI 10.1109/TCPMT.2018.2875460, IEEE Transactions on Components, Packaging and Manufacturing Technology

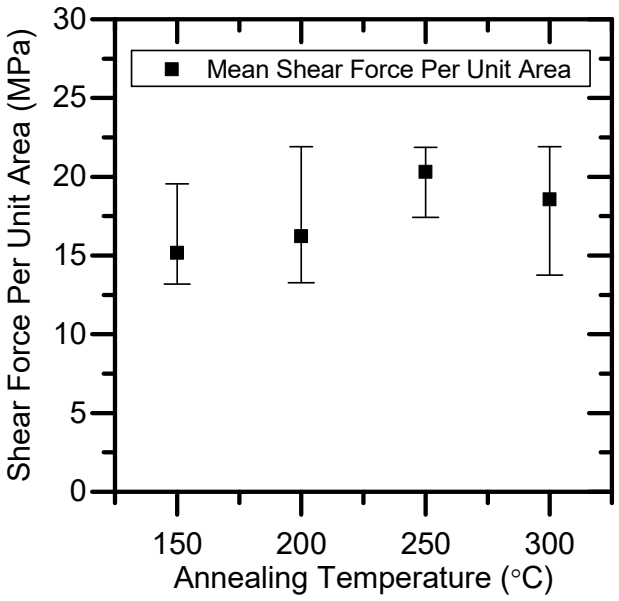

Fig. 11. Mean shear force per area with minimum and maximum values represented by error bars for different post-bonding annealing temperature

V. Cu-Cu Bonds Hermeticity Property

A. Experimental Procedure

To examine the hermeticity property of the bonded Cu, two 6" Si wafers (100) of 675 µm thickness were used as the substrates for the top and bottom dies. Deep reactive-ion etching (DRIE) was used to etch away 0.08 mm of Si leaving a sealing ring feature behind for each of the Si top die. The sealing ring feature, shown in Figure 12, forms a cavity volume of 1.24 mm^3, which is greater than the minimum required volume of 1 mm^3 for accurate helium (He) leak testing [18]. The sealing ring thickness is 0.15 mm and the distance from the edge to the sealing ring is 1 mm. The same thicknesses of SiO_2, Ti and Cu as the samples used in shear strength test were deposited on both the wafers. After the deposition of Cu, the wafers were diced into individual dies with the dimension showed in Figure 8. Each pair of top and bottom dies was activated by Ar/N_2 plasma. Average root mean square (RMS) roughness of the activated samples is 1.2 nm. Within 3 min after plasma activation, a bonding force of 385.24 N was applied to each sample for 5 min and the samples were annealed at temperature and duration same as those of the shear strength test.

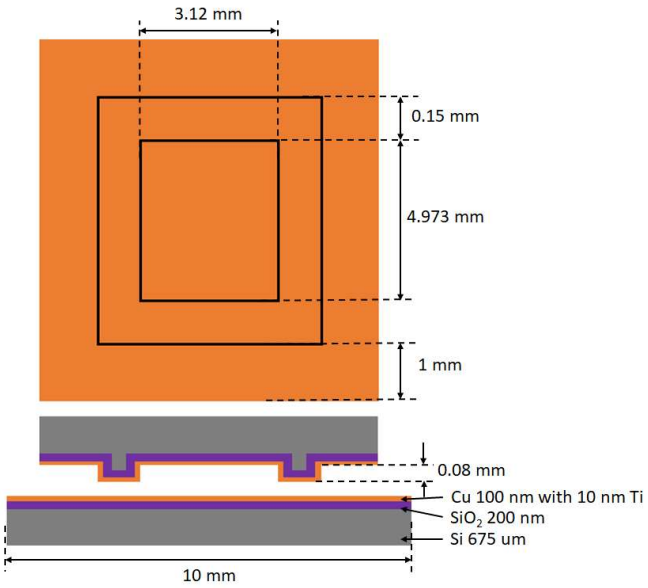

Fig. 12. Schematics of the top and bottom dies for fine leak test samples

During hermeticity examination, He leak test was first performed on the samples. The samples were placed in a bombing chamber with a gauge pressure of 0.52 MPa for 2 h as specified in the MIL-STD-883E standard and tested with a mass spectrometer for helium leak immediately upon removal from the bombing chamber [19].

After the fine leak test, a perfluorocarbon bubble gross leak test was performed for gross leak according to the MIL-STD-883E standard. The samples were firstly placed in vacuum at 5 torr for 30 min to evacuate the cavity. Subsequently the samples were submerged in Type I perfluorocarbon and placed in the bombing chamber at gauge pressure of 0.52 MPa for 2 h. Type I perfluorocarbon has a boiling point of 56 ºC. In the event that a die demonstrates gross leak, the Type I perfluorocarbon will penetrate the sealing ring and fill the cavity. After the bombing, the dies were removed from the Type I perfluorocarbon and air dried for 20 s. Then, the samples were placed in a heated tank of Type II perfluorocarbon (boiling point at 179 ºC) at 125 ºC. Air drying allowed the Type I perfluorocarbon on the die surface to evaporate prior to immersion in the Type II perfluorocarbon tank. Upon immersion in the tank, Type I perfluorocarbon within the cavity of the dies boiled and escaped from the cavity as bubbles. If the die did not have a gross leak, Type I perfluorocarbon will not be present in the cavity and therefore no bubbles will be observed.

The samples must satisfy both tests for acceptance of hermeticity. The requirement for the fine leak test is to have He leak rate less than 5×10^{-8} atm.cc/s, and the requirement for the gross leak test is to have no observable bubbles from the sealed cavity.

B. Results and Discussion

The results in Figure 13 on the hermeticty test show that samples annealed at 150 and 250 ºC are among the lowest in He leak rate. However, all the samples annealed at 150 ºC failed the bubble test. These contradicting results require careful

contextual analysis. The samples annealed at 150 ºC have the weakest mechanical strength and as a result the samples failed to retain the He trapped in the cavity when mass spectrometer chamber was pumped down before commencing the He leak test. Hence, very limited amount He was detected during the He leak test. Consistent with the shear test results, samples annealed at 250 ºC have the best hermetic sealing. The leak rate is observed to increase as the annealing temperature decreases as expected. Samples annealed at 300 ºC also have higher leak rate as compared to 250 ºC annealed samples possibly due to the higher amount of oxidation of the Ti layer that compromises the mechanical strength of the bonded Cu layer.

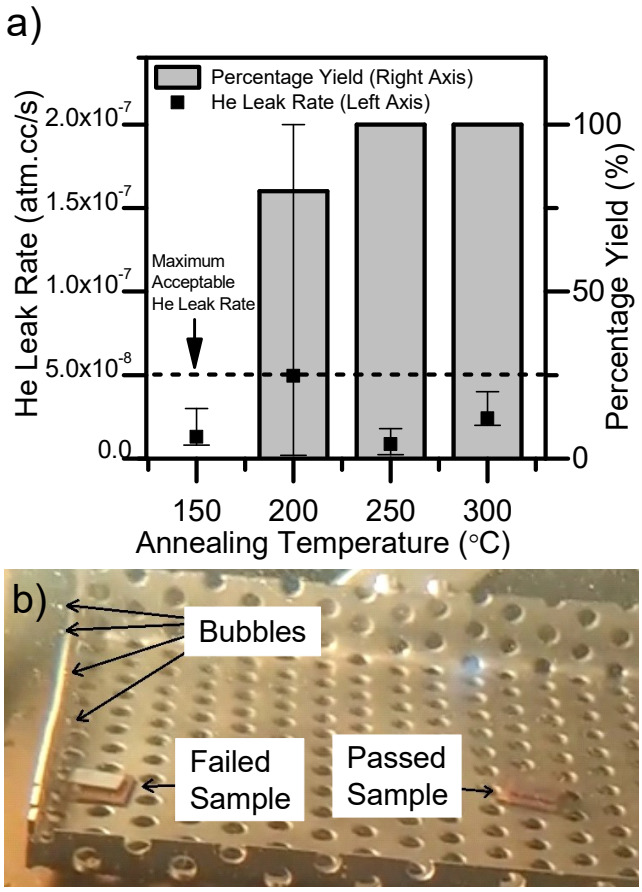

Fig. 13. a) Fine leak test results for different post-bonding annealing temperature and percentage yield (Total of 6 sample per anneal temperature). b) Image showing both passed and failed bubble test samples with bubble coming out of failed sample.

VI. Cu-Cu Bonds Electrical Property

A. Experimental Procedure

The electrical property of the bonded samples was studied by forming Daisy chain structures. RIE was performed on two 6" Si wafers (100) of 675 µm thickness to remove 6 µm of Si to form the Daisy chain structures as shown in Figure 14. After RIE, 200 nm of SiO_2 were deposited by TEOS PECVD. Lift-off process was used to pattern the 10 nm Ti and 100 nm Cu deposited on the SiO_2. After lift-off, the wafers were diced into top and bottom dies. The dies were activated by Ar/N_2 plasma and bonded within 5 min with a pick and place tool with alignment capability of 5 µm in accuracy. A bonding force of 210 N was applied to the sample for 5 min. Dummy samples with pre-connected Daisy was also fabricated for comparison with the bonded samples. These pre-connected dummy samples allowed for isolation of the root-causes (such as poor bonding, surface oxidation, etc.) that result in higher electrical contact resistance. The bonded sample, Ar/N_2 plasma activated dummy sample and non-activated dummy sample were annealed at 300 ºC for 2 h. The annealing temperature of 300 ºC was chosen as it caused the most oxidation in the metal layers as the worst case. After annealing, the samples were probed to measure the resistance of the Daisy chain at different interval.

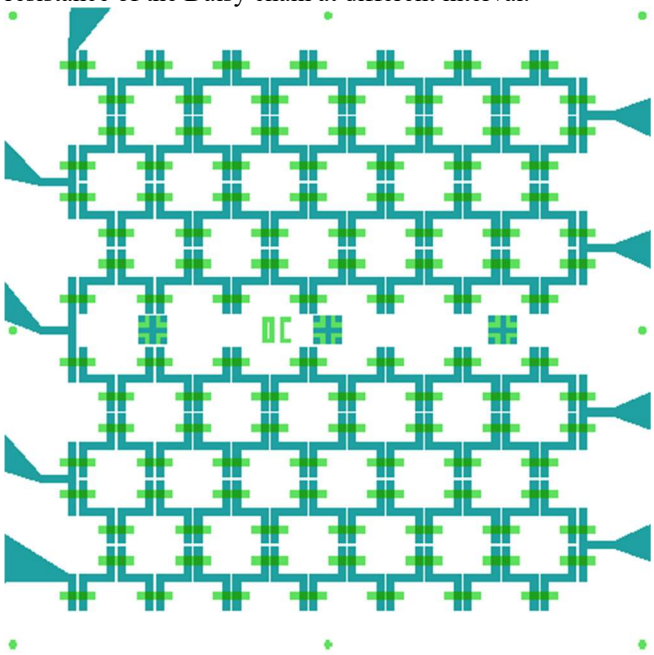

Fig. 14. Schematics of overlapping top and bottom Daisy chain design

Finally, temperature cycling test (TCT) ranging from -40 to 125 ºC was performed on the samples in atmospheric environment. The resistances for the bonded sample, activated dummy sample and the non-activated dummy sample were measured after 500 and 1,000 cycles of TCT, respectively.

B. Results and Discussion

Figure 15 shows the simplified schematics of the bonded sample, activated dummy sample and the non-activated dummy sample, their description and respective electrical test results.

Samples	Description	Results
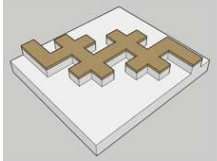 Dummy	Dummy sample with a single connected Cu pattern on SiO_2/Si structure	Before anneal: Fig.16a (Dummy) After Anneal: Fig.16a (Annealed Dummy) After Anneal and 500 TCT: Fig.16b (Dummy) After Anneal and 1000 TCT: Fig.16c (Dummy)
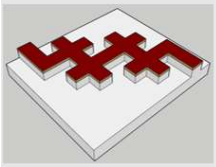 Activated Dummy	Activated dummy sample with a single connected Cu pattern on SiO_2/Si structure, processed with plasma activation	After Anneal: Fig.16a (Annealed Activated Dummy) After Anneal and 500 TCT: Fig.16b (Activated Dummy) After Anneal and 1000 TCT: Fig.16c (Activated Dummy)
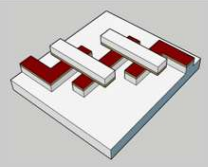 Bonded	Bonded sample with non-connecting patterned on bottom dies which will be connected by the patterns on top die	After Anneal: Fig.16a (Annealed Bonded Sample) After Anneal and 500 TCT: Fig.16b (Bonded Sample) After Anneal and 1000 TCT: Fig.16c (Bonded Sample)

Fig. 15. Simplified schematics of the bonded sample, activated dummy sample and the non-activated dummy sample.

Figures 16a, 16b and 16c show the Daisy chain resistance of the samples before TCT, after the 500 cycles TCT and after 1,000 cycles TCT, respectively. Dashed lines were drawn to represent best fitted linear lines. These show the variation of resistance at different segments of the Daisy chain. In principle, the Daisy chain resistance should be linear and intercepts the origin as every individual chain is designed to be identical. In Figure 16a, the annealed dummy sample (■) are of higher resistance compared to the non-annealed dummy sample (♦). This is due to oxidation of the Cu layers during annealing as the chamber for post bonding annealing contains some amount of residual O_2. On the other hand, the activated and annealed dummy sample (●) present a lower increase in the resistance. This suggests that the activation step helps to increase the oxidation resistance due to the formation of copper nitride as discussed earlier. However, the bonded sample (▲) shows the highest resistance compared to the other samples. It also shows deviation from the best fitted line. The higher resistance and deviation could be due to uneven bonding and misalignment between the top and bottom dies. Figure 17 shows the forcefully separated top and bottom dies after the one thousand cycles of TCT. Misalignment of approximately 32 µm can also be observed when compared to the design of the Daisy chain shown in Figure 14. The large misalignment of the dies was caused by the shifting of the bottom die when external bonding force is applied.

After 500 cycles of TCT, all samples' resistance increased as evidenced from Figure 16b, largely due to oxidation as the TCT was performed in ambient air. However, both the activated dummy (●) and bonded (▲) samples resistance are much higher than that of the dummy sample (■). This shows that the activation step increases the oxidation rate of Cu when the Cu surface is exposed to atmospheric air at elevated temperature. The bonded sample has the highest resistance and deviation from the best fitted line. In Figure 16c, after 1,000 cycles of TCT, further increase in resistance is clearly observed. The activated dummy sample (●) resistance was the highest with non-linear characteristic. Unlike the activated dummy samples (●), the bonded sample (▲) Cu surface was exposed only through small gaps between the top and bottom dies and the bonded area was not exposed. This reduces the oxidation rate as the air could not flow between the dies freely. However, the activated sample (●) was exposed completely during experiment, hence there was higher oxidation rate across the Daisy chains. Non-activated dummy samples (■) have the lowest resistance and least deviation from the best fitted line.

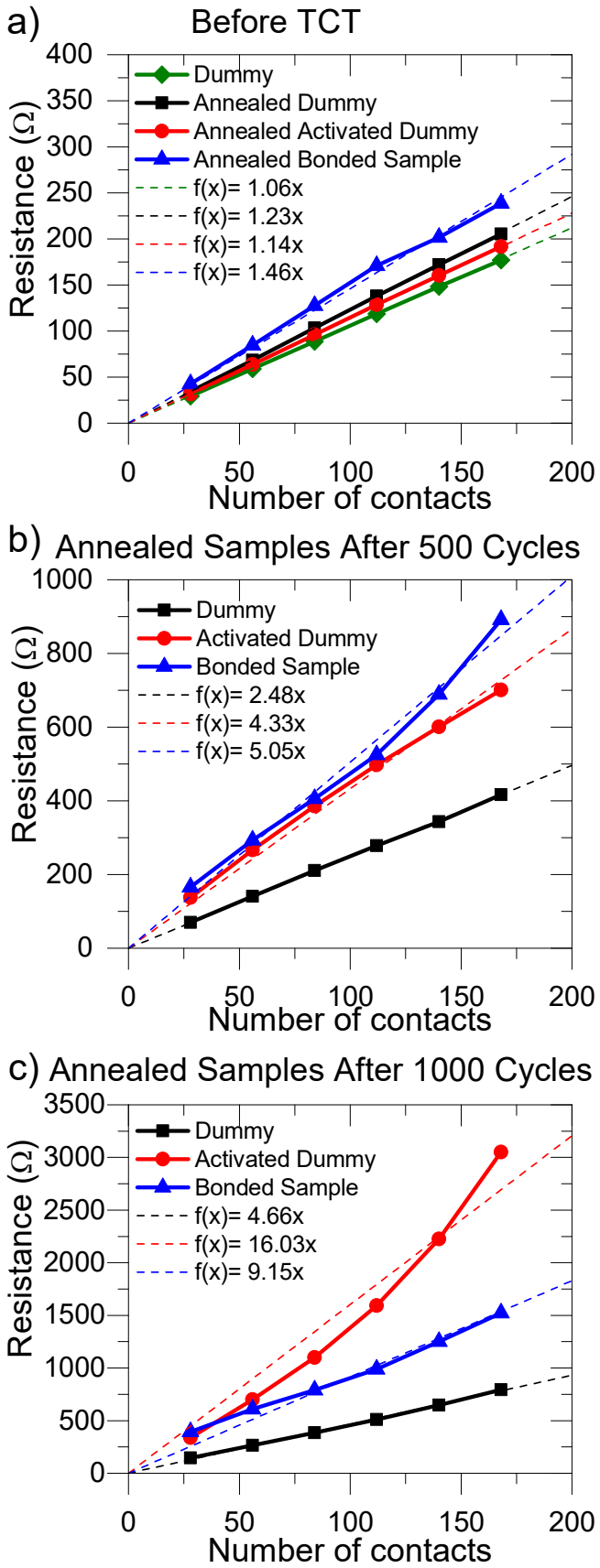

Fig. 16. Daisy chain resistance a) before TCT, b) after 500 cycles and c) after 1000 cycles.

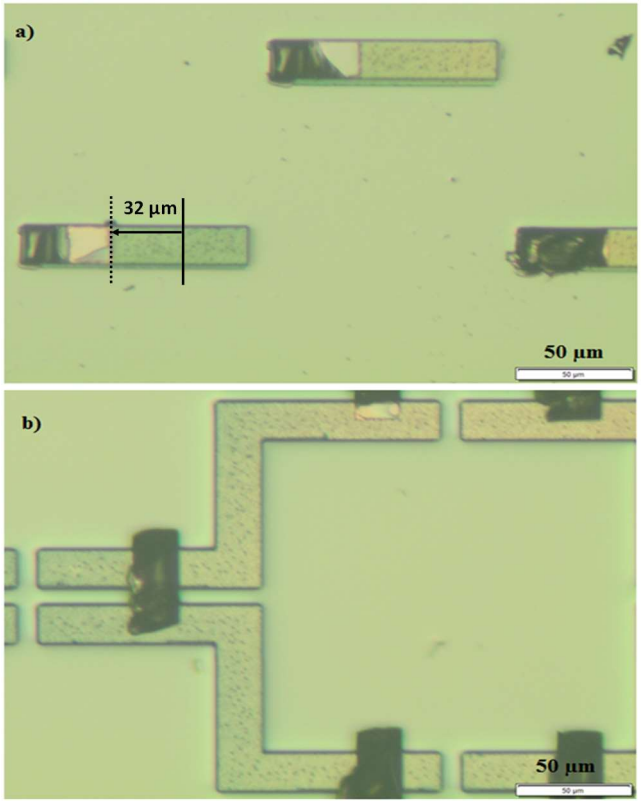

Fig. 17. Optical microscope image of separated a) top die with misalignment from original design and b) bottom die of bonded sample

After the TCT, the bottom die of the bonded sample and the non-activated dummy were further examined to understand the microstructure of the bonded layer by means of transmission electron microscopy and energy-dispersive X-ray spectroscopy (TEM/EDX) line scan. Figure 18 and figure 19 show the TEM/EDX line scan of non-activated dummy and bonded sample bottom die at the metal layers, respectively. The line scan in Figure 18 shows that the bonded sample have lower thickness of Cu layer as compared to the line scan in Figure 19. This shows that the oxidation rate of Cu is higher after activation. This increase in oxidation consumes larger amount of Cu and increases the resistance of the Daisy chain. A TEM image of the bonded sample in Figure 20 shows varying depth of oxidation along the metal line with one portion of Cu severely oxidized. This causes the large increase of resistance compared to the non-activated dummy sample.

This article has been accepted for publication in a future issue of this journal, but has not been fully edited. Content may change prior to final publication. Citation information: DOI 10.1109/TCPMT.2018.2875460, IEEE Transactions on Components, Packaging and Manufacturing Technology

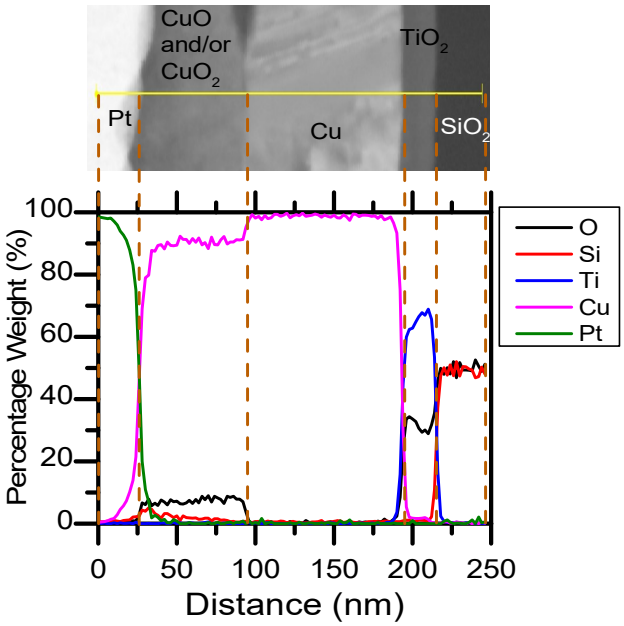

Fig. 18. TEM/EDX linescan of non-activated dummy sample at its metal layers after 1000 cycle TCT.

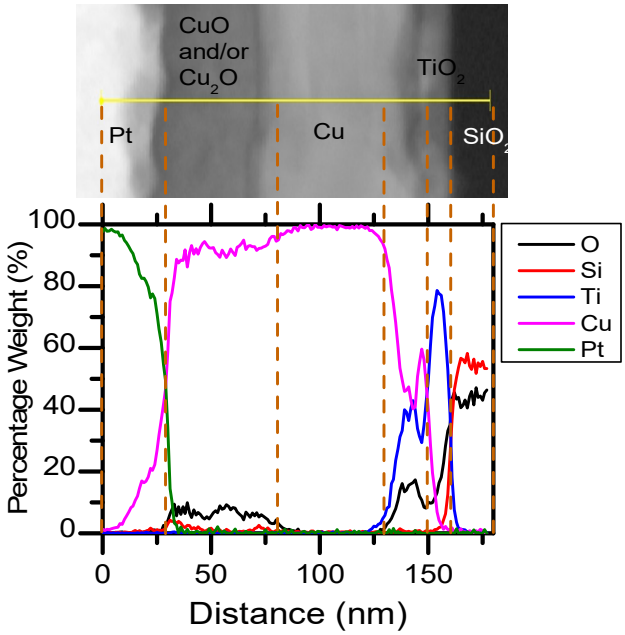

Fig. 19. TEM/EDX linescan of bonded sample bottom die at its metal layer after 1000 cycle TCT.

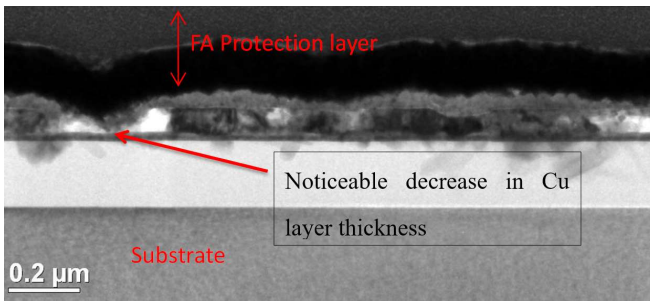

Fig. 20. TEM of bonded sample bottom die at its metal layers

It can also be observed that the TCT did not weaken the bonded sample as no bonding interface failure was observed when the sample was sheared and separated. In Figure 17 where the bonded sample was separated, the breakage of Si was observed. As the Daisy chain patterns were RIE etched into Si patterns, those patterns broke when the sample was forcefully separated. There was also delamination of Cu to Ti or Ti to Si interface observable on the separated dies. This was similar to the failure interface observed in the shear test samples for samples annealed at 300 ºC discussed earlier. The breaking of the Si patterns also shows that the Cu-Cu bond remains sufficiently strong after the TCT to withstand the shear force.

VII. Conclusion

In this work, a method was developed to bond Cu to Cu in ambient environment using Ar/N_2 plasma for surface cleaning and surface modification. Wafer level bonding with this method is also possible, however, die level bonding was demonstrated in this study to facilitate the characterization of the mechanical, hermeticity and electrical properties. Effects of post-bonding annealing temperature on shear strength and hermeticity were investigated. From the shear strength test and hermeticity test, samples annealed at 250 ºC had the highest average shear strength and lowest average leak rate. The shear strength and leak rate obtained at 250 ºC suggest that Cu-Cu direct bonding with Ar/N_2 plasma activation is a viable bonding technology for 3D packaging enabling greater number of components at a smaller foot print with shorter global interconnects that results in lower power consumption. However, the Daisy chain resistances of the TCT activated samples show that the activated Cu has higher oxidation rate as compared to non-activated Cu in ambient air. Passivation layers should be deposited to prevent exposure of Cu to the atmosphere as a mitigation. Cu-Cu bond does not fail during the TCT demonstrating that the Cu-Cu direct bonding with Ar/N_2 plasma surface activation method is able to provide mechanically reliable bond.

This method provides the following advantages.

1. Allows shorter bonding time as compared to thermocompression bonding and the ability to batch anneal. Actual bonding time is only 5 min while allowing multiple bonded samples to be annealed in batch at once in the annealing chamber since no force is required during the post-bonding annealing. This reduces time and energy to heat up each sample at a time in the case of thermocompression bonding.
2. Since the movement of Cu grain boundary from diffusion will increase the bonding strength, it is theoretically possible to anneal at a lower temperature for a longer time to achieve the bonding strength of a high temperature anneal. Low temperature post bonding anneal with longer duration will be investigated in future.
3. Cu-Cu bonds formed in wafer bonded sample do not have voids after 1000 TCT unlike SAC Cu pillar technology. Cu-Cu bonding allows smaller pitch size for interconnects compared to Cu pillar technology as the bonding occurs at solid phase.

4. This method also uses existing semiconductor fabrication equipment and requires only dry processes.

ACKNOWLEDGMENT

The authors wish to acknowledge support from Nanyang NanoFabrication Centre, NTU for help in fabrication of test samples. The authors also like to thank Jimmy Saputra and Almas Fachrullah from Excelitas Technologies for their help in the shear strength test, He fine leak test and bubble gross leak test.

REFERENCES

[1] P. Urard and M. Vučinić, "IoT Nodes: System-Level View", in *Enabling the Internet of Things: From Integrated Circuits to Integrated Systems*, M. Alioto, Editors, Cham, Switzerland, Springer International Publishing AG, 2017, p. 47-68.

[2] D. C. H. Yu, "New System-in-Package (SiP) Integration technologies," Proceedings of the IEEE 2014 Custom Integrated Circuits Conference, San Jose, CA, 2014, pp. 1-6.

[3] P. Gueguen, L. D. Cioccio, P. Gergaud, M. Rivoire, D. Scevola, M. Zussy, A. M. Charvet, L. Bally, D. Lafond and L. Clavelier, "Copper Direct-Bonding Characterization and Its Interests for 3D Integration", J. Electrochem. Soc., 156(10), H772 (2009).

[4] E. Higurashi, D. Chino and T. Suga, "Au–Au Surface-Activated Bonding and Its Application to Optical Microsensors with 3-D Structure," IEEE J. Sel. Top. Quantum Electron, 15(5), p1500 (2009)

[5] T. Suga, Y. Takahashi, H. Takagi, B. Gibbesch and G. Elssner, "Structure of AlAl and AlSi3N4 Interfaces Bonded at Room Temperature by Means of The Surface Activation Method," Acta Metall. Mater., 40 (Supp.) pS133-S137 (1992)

[6] N. Belov, T-K. Chou, J. Heck, K. Kornelsen, D. Spicer, S. Akhlaghi, M. Wang, T. Zhu, "Thin-Layer Au-Sn Solder Bonding Process for Wafer-Level Packaging, Electrical Interconnections and MEMS Applications," IEEE International Interconnect Technology Conference, Sapporo, Hokkaido, 2009, pp. 128-130.

[7] C. C. Lee, C. Y. Wang and G. Matijasevic, "Au-In bonding below the eutectic temperature," IEEE Transactions on Components, Hybrids, and Manufacturing Technology, 16(3), pp. 311-316, May 1993

[8] J. Fan, D. F. Lim, L. Peng, K. H. Li and C. S. Tan, "Low Temperature Cu-to-Cu Bonding for Wafer-Level Hermetic Encapsulation of 3D Microsystems", Electrochem. Solid-State Lett., 14(11), H470 (2011).

[9] A. Shigetou, T. Itoh and T. Suga, "Direct bonding of CMP-Cu films by surface activated bonding (SAB) method", J. Mater. Sci., 40(12), 3149 (2005).

[10] S. L. Chua, G. Y. Chong, Y. H. Lee and C. S. Tan, "Direct copper-copper wafer bonding with Ar/N2 plasma activation," 2015 IEEE International Conference on Electron Devices and Solid-State Circuits, Singapore, 2015, pp. 134-137.

[11] S. L. Chua and C. S. Tan, " Cu-Cu Die to Die Surface Activated Bonding in Atmospheric Environment Using Ar and Ar/N2 Plasma," ECS Trans., 75(9), p. 109-116 (2016)

[12] J. Yu, A. Anand, Y. Mui, P. Srinivasan and R. Master, "Reliability Study on Copper Pillar Bumping with Lead Free Solder," 2007 9th Electronics Packaging Technology Conference, Singapore, 2007, pp. 618-622.

[13] Y. Mishina and C. Herzig, "Grain boundary diffusion: recent progress and future research," Mater. Sci. Eng. A, 260(1-2), p55-71 (1999).

[14] B. Derby & E. R. Wallach, "Theoretical model for diffusion bonding," Metal Science, 16(1), p. 49-56 (1982)

[15] W. Gust, S. Mayer, A. Bögel and B. Predel, "Generalized Representation of Grain Boundary Self-Diffusion Data," J. Phys. Colloq., 46(C4), pp. 537-544 (1985).

[16] C. Y. Ting, M. Wittmer, S. S. Iyer and S. B. Brodsky, "Interaction between Ti and SiO_2," J. Electrochem. Soc., 131(12), p2934-2938 (1984)

[17] M. Takeyama, A. Noya, K. Sakanishi, H. Seki and K. Sasaki, " Solid-Phase Reactions of Diffusion Barriers of Ti and TiN to Copper Layers on SiO_2," Jpn. J. Appl. Phys. 35, 4027 (1996)

[18] Y. Tao and A. P. Malshe, "Theoretical Investigation on Hermeticity Testing of MEMS Packages Based on MIL-STD-883E," Microelectron Reliab, 45(3-4), p. 559-566 (2005).

[19] MIL-STD-883E, Method 1014.9, Test Method Standard: Micro-circuits, (1995).